International Journal of Adhesion & Adhesives 118 (2022) 103227

Contents lists available at ScienceDirect

International Journal of Adhesion and Adhesives

journal homepage: www.elsevier.com/locate/ijadhadh

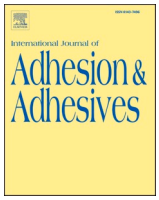

Elastic solutions for stresses in compliance-tailored adhesive anchors

M.A. Khan [e], B.L. Wardle [c,d], S. Kumar [a,b,*]

[a] James Watt School of Engineering, University of Glassgow, Glasgow, G12 8QQ, UK
[b] Glasgow Computational Engineering Center, University of Glasgow, Glasgow, G12 8LT, UK
[c] Department of Aeronautics & Astronautics, Massachusetts Institute of Technology, 77 Massachusetts Avenue, Cambridge, MA, 02139-4307, USA
[d] Department of Mechanical Engineering, Massachusetts Institute of Technology, 77 Massachusetts Avenue, Cambridge, MA, 02139-4307, USA
[e] Department of Civil Engineering, Mahindra University, Ecole Centrale School of Engineering, Bahadurpally, Hyderabad, 500043, India

ARTICLE INFO

Keywords:
Post-installed anchors
Boston tunnel
Compliance-tailored bondline
Pull-out performance
Bonded structures
Adhesive bonding

ABSTRACT

Joining of structures via adhesive anchors is of theoretical and practical engineering importance, including anchors that support concrete ceilings in urban infrastructure. Such anchors typically fail due to stress concentrations at the loaded and/or embedded ends, captured by the well-known 'shear-lag' model. Herein, such anchors are revisited by considering elastic properties variation of the adhesive along the embedment length in discrete steps, to reduce critical stress concentrations, and thereby minimize the propensity of failure. Initially, a closed-form solution is developed for a system with single-step variation in adhesive compliance along the embedment length (henceforth referred to as double-adhesive bondline), which agrees well with Finite Element simulations. The simplest double-adhesive tailoring is found to reduce the maximum shear stress by 43% while maintaining the super-critical bondlength characteristics of such designs. The theoretical framework thus developed is extended to systems comprising an arbitrary number of discrete adhesives along the embedment length considering, fixed and free boundary conditions of the embedded-end, to allow for parametric evaluation of the adhesive compliance tailoring for optimal stress reduction (maximum shear stress reduces by 46% for triple-adhesive bondline) while maintaining critical-length characteristics. The adhesive tailoring could be effectively applied to anchors with critical-length characteristics by employing a facile double-adhesive bondline with the compliant adhesive near the loaded-end and stiffer adhesive near the embedded-end. The particular case of the well-known Boston tunnel anchor problem is analyzed as an exemplary demonstration of the approach.

1. Introduction

Post-installed adhesive anchors find their applications in construction industry, anchor bridges and sealing [1]. They can also be used to anchor masonry units or rocks like limestone, basalt and sandstone [2]. Adhesively bonded anchors usually consist of a (steel) anchor bar inserted into a drilled hole in hardened concrete and thermosetting structural adhesive acting as a bonding agent between the concrete and the anchoring bar [3]. Colak et al. [4], reported considerable variations in the behavior of bonded anchors with bondline thickness and the choice of adhesive. There are four failure modes identified for steel anchors in concrete loaded in tension: 1. yielding of the (steel) anchor rod, 2. concrete-cone break out, 3. combined cone and bond failure and 4. bond failure [5]. The yielding of the anchor bar usually is observed for anchors with very large embedment lengths while the concrete-cone failure (usually brittle in nature), is observed in bonded anchors of very shallow embdements without an accompanying bond failure. For bonded anchors with larger embedment length, concrete failure accompanied by bond failure is most commonly observed [6–8]. The experimental data provided by Ref. [8], shows that the bond failure mode is usually observed at embedment length of about 8.3–10 times the diameter of the anchor, while the steel anchor bar failure mode is observed when embedment length is about 11.2 times the anchor diameter. These observations were made for systems with adhesive thickness in the order of 2–4 mm and are influenced by the moduli of the embedding concrete and the adhesive.

The load transfer in case of bonded anchors loaded in tension predominantly occurs by shearing of the lateral adhesive along embedment length. Recently, bond failure due to lack of creep compliance in adhesive was reported as the primary cause for the collapse of the ceiling of interstate I-90 connector tunnel project in Boston, Massachusetts, U.S.A [9]. The embedment length of a typical anchor, in the accident report

* Corresponding author. James Watt School of Engineering, University of Glassgow, Glasgow, G12 8QQ, UK.
E-mail addresses: msv.kumar@glasgow.ac.uk, s.kumar@eng.oxon.org (S. Kumar).

https://doi.org/10.1016/j.ijadhadh.2022.103227
Received 6 March 2022; Received in revised form 19 May 2022; Accepted 13 June 2022
Available online 15 July 2022

[9], was about eight times the diameter of the anchor bar, falling into the typical design where the entire load is transferred to the concrete over the anchor length through shearing of the adhesive, i.e., no load is designed to be carried at the embedded end. This length required to transfer the entire load in this manner is the critical length, and is governed by shear-lag theory [10,46,47]. In the context of bond failure (usually observed in anchors of larger embedment lengths), this length is a critical bondlength beyond which no further reduction in peak stress in the bondline is observed [11]. The critical bondlength is dependent on the geometric and material properties of anchorage system and is reported by challal et al. [12], as 10 times the diameter for glass fiber rods embedded in concrete and cement grout. The critical bondlength increases as the strength of the substrate decreases [13] and is found to be about 10 times the diameter of the anchor for the anchors embedded in the substrate such as low strength concrete [14]. Conventionally, such a transfer length for steel-concrete interface under tension is referred to as development length [15]. In the present study, the shear-transfer or development length is also referred to as critical-length.

Numerous theoretical, experimental and numerical investigations have been conducted on bonded anchors (see, for instance Refs. [5, 16–19]). Cohesive zone modeling (CZM) is often utilized to predict the failure, including interfacial failures in bonded systems using cohesive zone elements whose properties depend on experimental traction-separation laws [20,21]. For instance, CZM was utilized for modeling failure behavior of interfaces between aggregate and cement paste [22]. The experimental works of Cook et al. [5,23], and Doerr et al. [24], provided detailed insight into the failure behavior of adhesively bonded anchors. Shear-lag elastic analysis was extensively used to evaluate the non-uniform bond stress in the adhesively bonded anchors [6,17]. Wang [19] performed 3D elastic analyses of conventional bonded anchors and showed that the 1-D elastic solution predicts the load carrying capacity reasonably well for relatively stiff substrate like concrete. It was also reported that the 3D models are more suitable for anchors embedded in soft substructures such as soil and soft rocks. Analytical model incorporating bond-slip behavior was developed by Chen et al. [25], for cable anchors fully grouted with cement. Zheng et al. [26], developed analytical solution for non-linear pull-out response of fiber-reinforced-polymer rods embedded in the steel tube with the cement grout, based on the shear-lag analysis. Prieto et al. [27], reported that most of the analytical models assumed that the embedded-end of the anchor is fully detached from the concrete. Such an assumption may not be fully valid. Only a few analytical models in the literature thus far considered the in-tact embedded-end condition of the anchor [1,11,27,28].

Non-uniform bond stress models for anchors (see, for instance Refs. [10,11]) indicate that the steep shear stress gradient exists near the loaded-end of the anchor. As the bond failure usually initiates from the loaded-end, we propose the use of the compliant adhesive for the bondline near the loaded-end to mitigate the stress concentration while retaining stiffer adhesive near the embedded-end, so as to improve the load carrying capacity. The benefit of such compliance tailoring for the composite and metallic bonded joints has been demonstrated experimentally and numerically [29–34]. Results of these studies indicate that the stress concentration in the adhesive can be reduced by considering spatially step-wise or smoothly varying properties of the bondline for metallic/composite lap joints. Previous works of authors have demonstrated that, owing to reduction in peak stresses in stress concentration zones, materially-tailored joints exhibit superior load carrying capacity and toughness in comparison to non-tailored joints [35–38]. Authors, in their previous studies, have also demonstrated compliance tailoring of multilayers via additive manufacturing [39–41].

The compliance tailoring of bondline along the bondlength, considering single-step/multiple-step variation in modulus, is proposed and explored in this study, in the context of bonded anchors. Using the concept of compliance tailoring for bonded anchors, functional variation in modulus of the bondline along embedment length was previously proposed and explored by the authors, to reduce the peak stresses in the bondline [10]. The primary difference in the behavior of adhesively bonded anchors from other metal to metal/plastic/fiber-reinforced-plastic joints stems from the failure modes of the brittle substrate such as concrete-cone and combined concrete-cone bond failures which are influenced by the load-shared by the embedded-end. This emphasizes the importance of modeling the fixed embedded-end condition, disregarded by most of the models in the literature as discussed in Ref. [27]. However, to the authors' best knowledge, there has been no work where the bonded anchors load-transfer behavior is studied in the presence of double or multiple adhesives along the embedment length.

The objective of the proposed study is to develop a closed-form solution for stresses in bonded anchors employing multiple adhesives along the embedment length. In the first stage of modeling, 1-D axisymmetric closed-form elastic solution is developed based on shear-lag analysis of bonded anchors, considering a single-step variation in modulus along the bondline with embedded-end fixed or free. The baseline solution with which comparison is made is obtained from the shear-lag analysis of the anchors with uniform properties along the entire embedment length. The solution is then validated by the finite element results and the extant bond stress model [17]. The proposed double-adhesive bondline models are extended for the anchors with n-adhesive bondlines. The effect of compliant adhesive phase on the stress-state of the bondline and the load shared by the embedded-end is studied in detail for some reported anchor configurations. The mechanics of double-adhesive bondline anchors is parametrically analyzed to identify optimal length and modulus of the compliant phase. As discussed above, the failure of the Boston tunnel is due to creep failure of the adhesive anchor [9]. Therefore, it is important that the soft adhesive used in our analysis is as high creep resistant as the stiff adhesive in the bondline. On the other hand, if the creep resistance of the soft adhesive is lower than the stiff adhesive, we could still impose limit on the stress in the soft adhesive and design for lower stress in the soft one to stay under the limit. However, the analysis is still useful. Due to practical difficulties associated with the use of multiple adhesives along the bondline, we advocate the use of double-adhesive bondline. The analyses of anchors carried out later with various bondline configurations will be helpful for comparison in terms of peak stress reduction.

2. Analytical modeling

A typical anchor configuration reported in the interstate I90 tunnel in Boston [9], is reproduced in Fig. 1a. This typical anchor assembly is idealized here as an anchor of diameter d, embedded into a semi-infinite matrix over a depth l as shown in Fig. 1b and carries an axial tensile load P. An adhesive layer of thickness t with varying shear modulus along the embedment length $G(z)$ is surrounding the anchor and the diameter of hole is $d + 2t$. The elastic modulus of anchor is much higher compared to the adhesive, leading to negligible lateral deformation of the anchor bar under the load P. Let $w(z)$ be its deformation in the loading direction z, neglecting the Poisson's effect of the anchor. As discussed before, 1-D solution neglecting Poisson's ratio, could be employed for anchors with stiff matrix like concrete [19]. The axial strain ϵ and the axial stress σ, experienced by the anchor are

$$\epsilon = \frac{dw}{dz}, \sigma = \frac{dw}{dz}E \tag{1}$$

where, E is the elastic modulus of the anchor. The shear strain γ and the corresponding shear stress τ in the bondline are given, respectively, by

$$\gamma = \frac{w}{t}, \tau = \frac{w}{t}G(z) \tag{2}$$

The strain energy in the system, due to axial deformation of the anchor and the shear deformation of the adhesive can be expressed in the functional form as

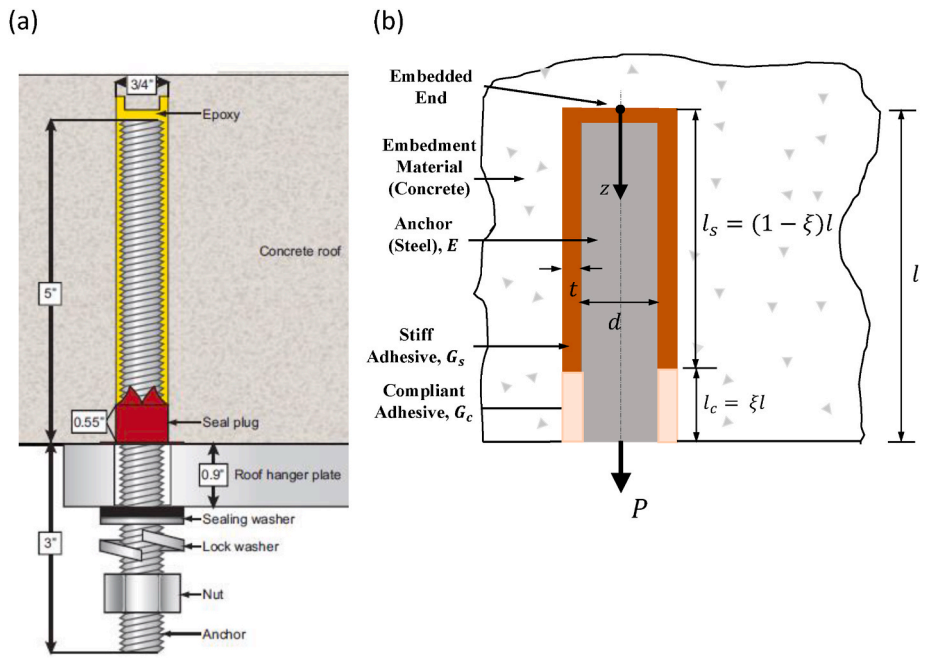

Fig. 1. (a) Typical configuration of an adhesive anchor in the interstate I90 tunnel [9]; (b) Idealization of the anchor embedded in the concrete ceiling with a double-adhesive bondline. G_s and G_c denote the shear moduli of stiff- and compliant-phase, respectively. l_s and l_c denote the lengths of stiff- and compliant-phase, of the adhesive, respectively. Note, $l_c = \xi l$ and $l_s = (1-\xi)l$.

$$U = \int_0^l \left(\frac{EA}{2} \left(\frac{dw}{dz} \right)^2 + \left(\frac{\pi(d+t)}{2t} \right) G(z) w^2 \right) dz \tag{3}$$

where, $A = \frac{\pi}{4}d^2$ is the cross-sectional area of the anchor. Using Euler-Lagrange's variational principle, the strain energy is rendered stationary to obtain the following governing ordinary differential equation (ODE):

$$\left(\frac{\pi(d+t)}{t} \right) G(z) w - EA \left(\frac{d^2 w}{dz^2} \right) = 0 \tag{4}$$

The above ODE accounts for an arbitrarily variation in shear modulus of the adhesive, $G(z)$. The objective here, however, is to find a solution of the governing ODE for the adhesive anchor with a double-adhesive bondline considering both free and fixed embedded-end conditions of the anchor. In subsequent sections, the single-adhesive bondline and double-adhesive bondline are referred to as SBL and DBL, respectively.

2.1. Single-adhesive bondline (SBL)

Using a shear-lag analysis akin to Refs. [10,17], we begin with a solution to the conventional adhesive anchors with SBL, treated here as a baseline case. For an anchor with SBL, the shear modulus of the adhesive along embedment length, remains constant i.e., $G(z) = G$. The governing ODE, given by Eqn. (4), is accordingly simplified to

$$\left(\frac{\pi(d+t)}{t} G \right) w - EA \left(\frac{d^2 w}{dz^2} \right) = 0 \tag{5}$$

A general solution to the above second order ODE in closed-form is given by

$$w = C_1 \cosh(\alpha z) + C_2 \sinh(\alpha z) \tag{6}$$

where, C_1 and C_2 are the constants of integration and the constant $\alpha = \sqrt{\frac{\pi(d+t)G}{EAt}}$.

2.1.1. SBL: Free embedded-end

In case of SBL with free embedded-end, boundary conditions can be written as

$$\left. \frac{dw}{dz} \right|_{z=0} = 0; \quad \left. \frac{dw}{dz} \right|_{z=l} = \frac{P}{EA} \tag{7}$$

Applying the above boundary conditions to solution given by Eqn. (6), we obtain $C_1 = \frac{P}{EA\alpha} \frac{1}{\sinh(\alpha l)}$ and $C_2 = 0$. Therefore, the shear stress distribution in the adhesive along the bondline is obtained as:

$$\tau(z) = \left(\frac{P}{EA\alpha} \frac{G}{t} \right) \frac{\cosh(\alpha z)}{\sinh(\alpha l)} \tag{8}$$

From the above equation, we can see that, at the embedded-end, the shear stress is minimum and is equal to

$$\tau(0) = \tau_{min} = \left(\frac{P}{EA\alpha} \frac{G}{t} \right) \frac{1}{\sinh(\alpha l)} \tag{9}$$

For longer embedment length, as $\alpha l \to \infty$, we observe that the shear stress in the bondline at the embedded-end goes to zero. Similarly, the maximum shear stress in the adhesive occurs at the loaded-end and is equal to

$$\tau(l) = \tau_{max} = \left(\frac{P}{EA\alpha} \frac{G}{t} \right) \coth(\alpha l) \tag{10}$$

Note that for a very large l, the shear stress at the loaded-end i. e., $z = l$, becomes

$$\tau_{max}|_{l \to \infty} = \left(\frac{P}{EA\alpha} \frac{G}{t} \right) \tag{11}$$

Upon simplification, the axial stress in the anchor with free embedded-end, is obtained as

$$\sigma(z) = \left(\frac{P}{A} \right) \frac{\sinh(\alpha z)}{\sinh(\alpha l)} \tag{12}$$

2.1.2. SBL: Fixed embedded-end

In case of SBL with fixed embedded-end, the boundary conditions can be written as

$$w(0) = 0; \quad \left.\frac{dw}{dz}\right|_{z=l} = \frac{P}{EA} \tag{13}$$

Applying the above boundary conditions in Eqn. (6), we get $C_1 = 0$ and $C_2 = \frac{P}{EA\alpha}\frac{1}{\cosh(\alpha l)}$. The adhesive shear stress distribution along the bondline can be obtained as

$$\tau(z) = \left(\frac{P}{EA\alpha}\frac{G}{t}\right)\frac{\sinh(\alpha z)}{\cosh(\alpha l)} \tag{14}$$

Note that for the embedded-end fixed, shear stress is zero at the embedded-end. The maximum shear stress in the adhesive at the loaded-end is found as

$$\tau(l) = \tau_{max} = \left(\frac{P}{EA\alpha}\frac{G}{t}\right)\tanh(\alpha l) \tag{15}$$

Note that for a very large l, the maximum shear stress at the loaded-end i. e., $z = l$, becomes

$$\tau_{max}|_{l\to\infty} = \left(\frac{P}{EA\alpha}\frac{G}{t}\right) \tag{16}$$

Comparing Eqns. (11) and (16), we see that the influence of embedded-end boundary condition disappears for very large l i.e., the entire load is transferred through shearing of the bondline. Practically, such large embedment length is referred to as critical stress-transfer-length (l_{cr}), an important design parameter for such systems. The load shared by the embedded-end is evaluated using fixed boundary conditions. The axial stress in anchor for the fixed-end condition is obtained as

$$\sigma = \left(\frac{P}{A}\right)\frac{\cosh(\alpha z)}{\cosh(\alpha l)} \tag{17}$$

2.2. Double-adhesive bondline (DBL): Closed-form solution

A closed-form solution for the shear stress distribution in the anchor assembly with DBL is obtained by modeling a step-change in shear stiffness of the bondline such that

$$G(z) = \left\{\begin{array}{ll} G_s & 0 \le z \le (1-\xi)l, \\ G_c & (1-\xi)l \le z \le l \end{array}\right| \; z \in [0, l] \tag{18}$$

where, G_c and G_s are the shear moduli of the compliant- and the stiff-phase of the bondline, respectively, l_s and l_c are the lengths of the stiff and the compliant adhesives, respectively, and $\xi = l_c/l$ is the compliant bondlength ratio denoting the length of compliant phase with respect to the embedment length l, as seen in Fig. 1b. Using the DBL shear modulus profile given by Eqn. (18), the general solution to the ODE given by Eqn. (4), can be written as

$$w(z) = \left\{\begin{array}{ll} C_1\cosh(\alpha_1 z) + C_2\sinh(\alpha_1 z); & 0 \le z \le (1-\xi)l, \\ C_3\cosh(\alpha_2 z) + C_4\sinh(\alpha_2 z); & (1-\xi)l \le z \le l \end{array}\right. \tag{19}$$

Therefore, the shear stress in the compliant- and the stiff-phase of the bondline, respectively, is found to be

$$\tau(z) = \left\{\begin{array}{ll} (C_1\cosh(\alpha_1 z) + C_2\sinh(\alpha_1 z))\frac{G_s}{t}; & 0 \le z \le (1-\xi)l, \\ (C_3\cosh(\alpha_2 z) + C_4\sinh(\alpha_2 z))\frac{G_c}{t}; & (1-\xi)l \le z \le l \end{array}\right. \tag{20}$$

And the corresponding the axial stress distribution in the anchor is given by

$$\sigma(z) = \left\{\begin{array}{ll} (C_1\sinh(\alpha_1 z) + C_2\cosh(\alpha_1 z))E\alpha_1; & 0 \le z \le (1-\xi)l, \\ (C_3\sinh(\alpha_2 z) + C_4\cosh(\alpha_2 z))E\alpha_2; & (1-\xi)l \le z \le l \end{array}\right. \tag{21}$$

The peak stress in the stiff and compliant adhesives occurs either at the interface (at which step-change in shear modulus is provided) or at the free surface of the compliant adhesive near the loaded-end, respectively. Therefore, these peaks are obtained as

$$\tau_{max}|_s = C_1\cosh(\alpha_1(1-\xi)l)\frac{G_s}{t} + C_2\sinh(\alpha_1(1-\xi)l)\frac{G_s}{t} \tag{22}$$

$$\tau_{max}|_c = (C_3\cosh(\alpha_2 l) + C_4\sinh(\alpha_2 l))\frac{G_c}{t} \tag{23}$$

The peak stress in the bondline is the maximum of the above two. Depending on the relative values of the constants α_1, α_2 and ξ, it occurs either in the stiff or compliant phase. Therefore, while performing parametric study, the magnitude of peak stresses and the locations at which they occur are explored for varying compliant bondlength ratio ξ and the factor $G_c/G_s = \alpha_1/\alpha_2$. In subsequent formulation, particular solutions are derived for the fixed and free embedded-end conditions.

2.2.1. DBL: Free embedded-end

From the compatibility of deformation along the embedment length of the bondline and the traction-free condition at the embedded-end, the solution given in the Eqn. (19) has to satisfy:

$$\begin{gathered} \left.\frac{dw}{dz}\right|_{z=0} = 0; \quad \left.\frac{dw}{dz}\right|_{z=l} = \frac{P}{EA}; \\ w(z=(1-\xi)l^-) = w(z=(1-\xi)l^+); \quad \left.\frac{dw}{dz}\right|_{z=(1-\xi)l^-} = \left.\frac{dw}{dz}\right|_{z=(1-\xi)l^+} \end{gathered} \tag{24}$$

The constants of integration C_1, C_2, C_3 and C_4 are determined by imposing the above boundary conditions to the general solution given by Eqn. (19) and are obtained as

$$\begin{gathered} C_1 = \frac{C_3\cosh(\alpha_2(1-\xi)l) + C_4\sinh(\alpha_2(1-\xi)l)}{\cosh(\alpha_1(1-\xi)l)}; C_2 = 0; C_3 = -\frac{K_2}{K_1}C_4; \\ C_4 = \frac{P}{EA}\left(\frac{K_1}{\alpha_2\sinh(\alpha_2 l)(K_1\coth(\alpha_2 l) - K_2)}\right) \end{gathered} \tag{25}$$

where,

$$\begin{aligned} K_1 &= \alpha_1\sinh(\alpha_1(1-\xi)l)\cosh(\alpha_2(1-\xi)l) - \alpha_2\cosh(\alpha_1(1-\xi)l)\sinh(\alpha_2(1-\xi)l) \\ K_2 &= \alpha_1\sinh(\alpha_1(1-\xi)l)\sinh(\alpha_2(1-\xi)l) - \alpha_2\cosh(\alpha_1(1-\xi)l)\cosh(\alpha_2(1-\xi)l) \end{aligned}$$

2.2.2. DBL: Fixed embedded-end

Again considering compatibility of deformation as before along the length of the bondline and the fixity of the embedded-end, the solution given in the Eqn. (19) has to satisfy:

$$\begin{gathered} w(0) = 0; \quad \frac{dw}{dz}_{z=l} = \frac{P}{AE}; \\ w(z=(1-\xi)l^-) = w(z=(1-\xi)l^+); \quad \left.\frac{dw}{dz}\right|_{z=(1-\xi)l^-} = \left.\frac{dw}{dz}\right|_{z=(1-\xi)l^+}; \end{gathered} \tag{26}$$

The constants of integration C_1, C_2, C_3 and C_4 are determined by applying the above boundary conditions on the general solution given by Eqn. (19). These constants are obtained as:

$$\begin{gathered} C_1 = 0; C_2 = \frac{C_3\cosh(\alpha_2(1-\xi)l) + C_4\sinh(\alpha_2(1-\xi)l)}{\sinh(\alpha_1(1-\xi)l)}; C_3 = -\frac{K_2}{K_1}C_4; \\ C_4 = \frac{P}{EA}\left(\frac{K_1}{\alpha_2\sinh(\alpha_2 l)(K_1\coth(\alpha_2 l) - K_2)}\right) \end{gathered} \tag{27}$$

where,

$$\begin{aligned} K_1 &= \alpha_1\cosh(\alpha_1(1-\xi)l)\cosh(\alpha_2(1-\xi)l) - \alpha_2\sinh(\alpha_1(1-\xi)l)\sinh(\alpha_2(1-\xi)l) \\ K_2 &= \alpha_1\cosh(\alpha_1(1-\xi)l)\sinh(\alpha_2(1-\xi)l) - \alpha_2\sinh(\alpha_1(1-\xi)l)\cosh(\alpha_2(1-\xi)l) \end{aligned}$$

2.2.3. Validation of the proposed DBL closed-form solution

For validation of the proposed models, we choose the configuration of Farmer's work [17] with SBL anchors as this original work was

validated by experiments. We also compare our analytical solutions with Finite Element (FE) results. In this example, the Poisson' ratio of the adhesive ν, not reported by Farmer, is assumed to be 0.4; the shear modulus of the compliant adhesive is taken as $G_c = 0.25G_s$; and the compliant bondlength ratio ξ was chosen to be 0.2. See Table 1 for the geometric and material properties of Farmer's configuration used here for validation. Table 1 also reports the computed load shared by the fixed embedded-end and a constant k_l relevant for discussing the critical length characteristics of anchors (see appendix section 5.2). Fig. 2a and b, shows the comparison of the stresses obtained from the proposed model for SBL and DBL assemblies against the FE results and the Farmer's solution [17], for the free and fixed embedded-ends, respectively. Note that the Farmer's solution is only valid for the free embedded-end condition as is the case with most of the theoretical models reported in literature [27]. We can see that the predicted axial and shear stress distributions match very well with the FE results and the Farmer's solution. The discrepancy in the shear stress prediction in comparison to the FE solution is within 2–5%. The inset in Fig. 2a shows that the traction-free condition i.e., zero axial stress at the embedded-end is exactly satisfied by the proposed model and the FE results. Further, the shear stress in the bondline with the free embedded-end condition agrees with the Farmer's solution (see Fig. 2a bottom panel). We also observe a reduction in peak shear stress, at the loaded-end by about 35% by employing DBL in lieu of SBL. From the inset shown in Fig. 2b, we can see that the shear stress reaches zero owing to fixed embedded-end condition. However, when the embedded-end is fixed, axial stress is noted at this end, signifying that a fraction of applied load is transferred through this embedded-end of the anchor, directly in tension to the matrix. We particularly emphasize on the load share/fraction at the embedded-end instead of axial stress due to uncertainty associated with fixity, depending upon the amount of adhesive reaching this end. The fraction of the load at the embedded-end is not significant for anchors with large embedment lengths. From comparisons of Fig. 2a and b and analyses carried out in Appendix 5.2, at the embedded-end, the adhesive shear stress for an adhesive anchor with free embedded-end is proportional to the axial stress for the anchor with fixed embedded-end. For large embedment lengths, the effect of the boundary condition manifested by the shear and axial stresses, near the embedded-end, vanishes as can be observed from the comparison between insets of Fig. 2. The closed-form expressions for the load-transfer at the embedded-end are presented in the subsequent sections for the anchors with SBL and DBL.

Table 1
Geometric and material properties of adhesive anchors tested or analyzed in previous works [5,17,24,27,42]. Prieto's anchor configuration [43] is derived from the Boston tunnel [9].*values are assumed for a structural adhesive [44]. The parameters p and k_l quantify the critical-length characteristics of adhesive anchor. **Bold** indicates the cases analyzed herein.

Properties	Farmer's **SBL** [17]	Cook's **SBL** [5]	Doer's SBL [24]	Prieto's SBL [27]
Embedment length l, mm	350	{ 88.9, 127, **177.8**}	{50.8, 101.6, 152.4}	127
Anchor diameter d, mm	20	{12.7, 15.9, **19**}	15.9	15.9
Anchor modulus E, GPa	180	210	210	210
Adhesive thickness t, mm	4	{ 0.8, **1.6**}	1.6	1.55
Adhesive modulus E_s, GPa	2.25	3.92*	3.92*	3.92
Poisson' ratio of adhesive	0.4*	0.4*	0.4*	0.4
Load shared by the fixed embedded-end p	0.66%	**0.9%**–2.7%	1.1%–34.45%	2.5%
Dimensionless constant, $k_l = \alpha l$	5.46	**4.3**–5.5	1.7–5.2	4.73

2.3. Load shared by the embedded-end: SBL and DBL

Let S and P_a be the load transferred through shearing of the adhesive along the bondlength and the tensile load resisted by the anchor, respectively, such that the applied load is written as

$$P = S + P_a = (1-p)P + pP; 0 \le p \le 1 \tag{28}$$

where, p is the fraction of load shared by the embedded-end. $p = 0$ for the free embedded-end condition. The load transferred through shearing of bondline S, is evaluated from the shear stress distribution $\tau(z)$ as $S = \pi(d + t)\int_0^l \tau(z)dz$. Upon simplification, for SBL anchor, we get load transferred by the bondline and the anchor at the fixed embedded-end, respectively, are

$$S = P(1 - \mathrm{sech}(\alpha l)); P_a = P\mathrm{sech}(\alpha l) \tag{29}$$

Note for theoretically very large value of l, $S = P$ and $P_a = 0$. Therefore, the proportion of load taken up by the embedded-end for the SBL anchor as a function of embedded length is given as

$$p = sech(\alpha l) \tag{30}$$

An important dimensionless constant which depends on the geometric and material properties of the anchor assembly, in order to identify critical-length characteristics is identified here as

$$k_l = \alpha l = l\sqrt{\frac{\pi(d+t)G}{AEt}} \tag{31}$$

In the above equation, the ratio $d/A \propto 1/d$ and hence anchors placed in groups, instead of single anchor is more effective in sharing the load. Larger diameter anchors have shown poor performance as per Cusens et al., [45]. Additionally, note that the larger embedment length l and smaller bondline thickness t help in increasing k_l. Previous studies have associated the aspect ratio l/d with the failure modes or the load-transfer characteristics (see, for instance Ref. [8]). However, we propose the use of constant k_l to characterize the load-tranfer behavior of bonded anchors. From Eqns. (30) and (31), p and k_l become significant when the anchor length is restricted, however, we focus our study on larger length anchors. Extending this approach, the load shared in shear by the DBL anchor is evaluated from the shear stress distribution $\tau(z)$ as $S = \pi(d + t)\int_0^l \tau(z)dz$, where, τ_z is obtained from Eqn. (20) along with the respective constants for the fixed embedded-end. Upon simplification, the proportion of load shared by the DBL anchor in tensile mode is formulated as

$$p = 1 - \pi(d+t)\left(\frac{K_2^*}{\alpha_1}(\cosh(\alpha_1 l(1-\xi)) - 1) + \frac{K_3^*}{\alpha_2}(\sinh(\alpha_2 l) - \sinh(\alpha_2 l(1-\xi))) + \frac{K_4^*}{\alpha_2}(\cosh(\alpha_2 l) - \cosh(\alpha_2 l(1-\xi)))\right) \tag{32}$$

where, $K_2^* = \frac{K_2}{P}, K_3^* = \frac{K_3}{P}$ and $K_4^* = \frac{K_4}{P}$ are the normalized constants which are independent of the applied load. From Eqn. (30), decreasing the shear modulus of adhesive will reduce the critical-length parameter k_l, leading to a larger proportion of load shared by the embedded-end. Therefore, we apply a selective treatment of bondline such that the reduction in the modulus does not significantly influence the load shared by the embedded-end.

2.4. n-adhesive bondline (nBL)

In this section, we extended the idea of step-wise compliance grading

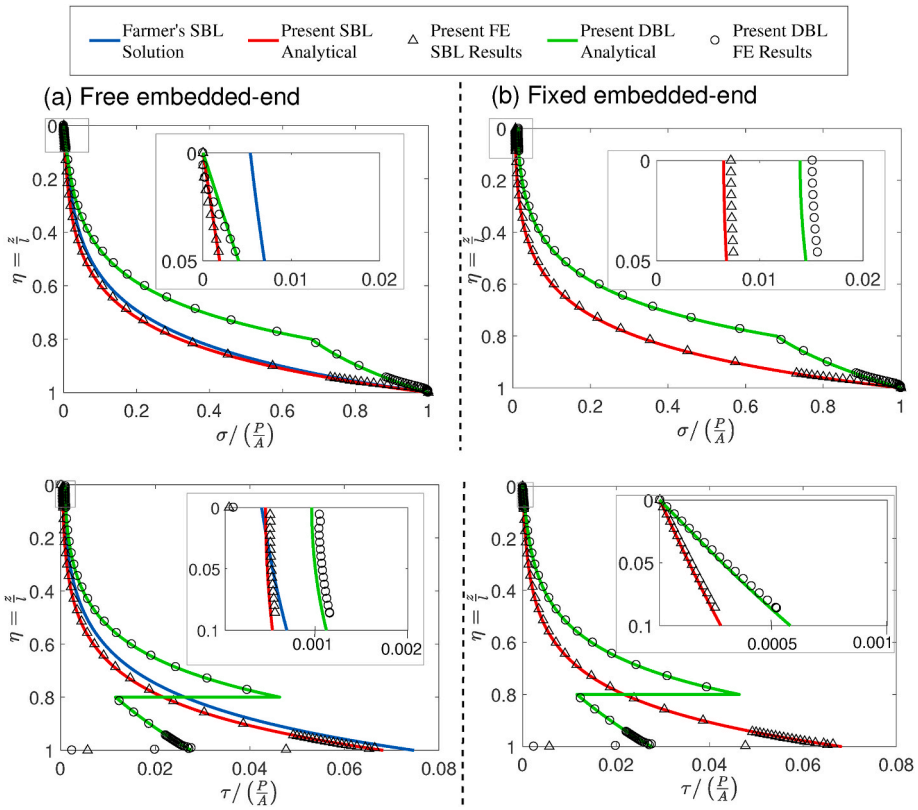

Fig. 2. Validation of proposed solution against the Farmer's solution [17] and the Finite Element results: Normalized axial stress in the anchor and adhesive shear stress distribution the single- and double-adhesive bondline anchors for (a) free embedded-end; and (b) fixed embedded-end. The insets depict the stresses near the embedded-end. $G_c = 0.25G_s$ and $\xi = 0.2$.

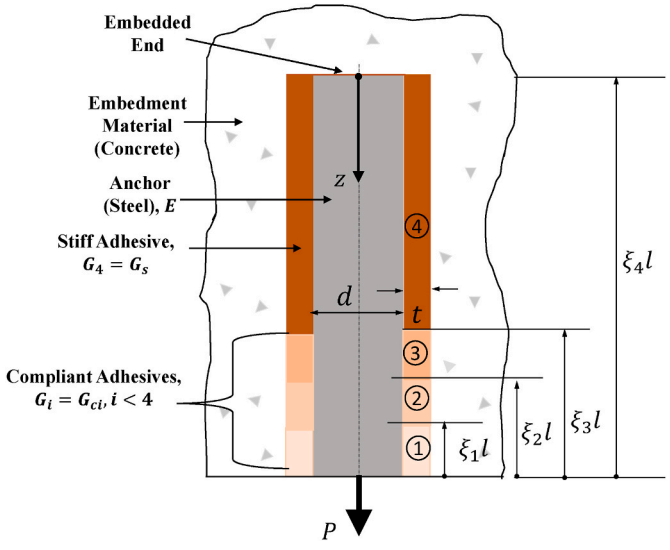

Fig. 3. Multi-adhesive bondline: Idealization of the adhesive anchor embedded into concrete ceiling, showing four adhesives in the bondline as exemplary that can be extended to visualize n-adhesive bondline. The compliant phase comprises three adhesives and the last phase contains stiff adhesive. Note that $\xi_4 = 1$.

to develop a framework for multi-adhesive bondline whose compliance changes in n number of discrete steps along the embedment length, referred here as nBL. The discrete adhesives, in this case, are arranged along the embedment length such that the nBL has decreasing compliance towards the embedded-end. Fig. 3 shows four discrete adhesives in the bondline. For multiple adhesives (say n) along the bondline, the solution in terms of the deformation of anchor for the governing ODE given by Eqn. (4), for the region i is given by

$$w_i(z) = K_i\cosh(\alpha_i z) + J_i\sinh(\alpha_i z); \zeta_{i-1} l \le z \le \zeta_i l \tag{33}$$

where, $i = 1, 2, \cdots n$, $\zeta_i = 1 - \xi_i$, $\alpha_i = \sqrt{\frac{\pi(d+t)G_i}{EAt}}$, K_i and J_i are constants, G_i is the shear modulus of phase i. In Fig. 3, $n = 4$ and $\xi_n = 1$. For coherence of discussions, we denote $G_{ic} = G_i$ for $n < i$ i.e., multiple complaint adhesives with $G_n = G_s$ for the stiff phase near the embedded-end. For n-adhesive bondline, from Fig. 3, we can see that G_{1c} is the modulus of the phase-1 which is at the loaded-end. Strategically, we employ the most compliant adhesive in this region and the modulus of adhesive chosen is increased as we approach a region closer to embedded-end. This strategy is based on previous work of the authors [10] and is implemented in a parametric optimization study discussed later. The adhesive which is placed at the embedded-end is chosen to be the stiffest adhesive with largest bondlength ratio. The larger bondlength ratio of stiffest phase would ensure effective load-transfer through the bondline, reducing stresses near the loaded-end. The displacement fields given in the above Eqn. (33) for the n regions will have $2n$ unknowns. The continuity of displacement at any interface $w_i((1-\xi_i)l) = w_{i+1}((1-\xi_i)l)$ gives us $(n-1)$ equations as follows

$$K_i\cosh(\alpha_i\zeta_i l) + J_i\sinh(\alpha_i\zeta_i l) - K_{i+1}\cosh(\alpha_{i+1}\zeta_i l) - J_{i+1}\sinh(\alpha_{i+1}\zeta_i l) = 0 \tag{34}$$

where, $i = 1, 2, \cdots (n-1)$. The continuity of first derivative of displacement along the bondline i.e., $w_i'(\zeta_i l) = w_{i+1}'(\zeta_i l)$ gives us another $(n-1)$ equations as follows

$$K_i\alpha_i\sinh(\alpha_i\zeta_i l) + J_i\alpha_i\cosh(\alpha_i\zeta_i l) - K_{i+1}\alpha_{i+1}\sinh(\alpha_{i+1}\zeta_i l) - J_{i+1}\alpha_{i+1}\cosh(\alpha_{i+1}\zeta_i l) = 0 \quad (35)$$

where, $i = 1, 2, \cdots (n-1)$. The boundary condition at the loaded-end i.e, $w_1'(0) = \frac{P}{AE}$ is substituted into Eqn. (33) to obtain

$$J_1 = \frac{P}{AE\cosh(\alpha_1 l)} \quad (36)$$

Thus we obtain $(2n-1)$ equations for $2n$ unknowns and the last constraint equation depends on the embedded-end condition. For the anchor with free embedded-end, the solution is obtained by solving Eqn. (34) – (36) along with $w_n = 0$ i.e., $J_n = 0$. For the anchors with fixed embedded-end, the solution is obtained by solving Eqn. (34) – (36) along with w_n' i.e., $K_n = 0$. We obtain a system of linear equations which are coded in MATLAB R2017a to solve for the unknown constants. Using the obtained constants, K_i and J_i, the shear stress in each of the adhesives is obtained as

$$\tau_i(z) = \frac{G_i}{t}(K_i\cosh(\alpha_i z) + J_i\sinh(\alpha_i z)); \zeta_{i-1} l \le z \le \zeta_i l \quad (37)$$

The fraction of load shared by the embedded-end p could be calculated by deducing the load shared by the bondline obtained from the above shear stress distribution. Therefore, $p = \frac{P-S}{P}$, where $S = \pi(d + t)\sum_{i=1}^{n}\int \tau_i dz$.

3. Results and discussion

To get a detailed insight into the mechanics of anchors bonded with DBL, we look at the practically adopted configurations of the SBL anchors, tested and analyzed by Cook [5,24] and are listed in Table 1. Cook and Doerr's original work reported bond properties evaluated from experiments. Note that the Boston tunnel geometry is a subset of the configuration tested by Cook. We further classify the reported anchors into short, critical-length and super-critical-length anchors. The anchors with 50 mm length are classified as short and the anchors with 177.8 mm as super-critical-length anchors. Critical/development length, as discussed before, is the minimum length required to allow full stress transfer in shear mode. From the analysis discussed later, we note that the anchor with 127 mm bondlength is a critical-length anchor. The critical-length is identified from stress analyses [10] and, as discussed before, is dependent on the shear stiffness of the bondline. Changing the shear modulus/stiffness could lead to a loss of critical-length characteristics, e.g., increased adhesive compliance causes the required critical length to increase. This is discussed in appendix section 5.2.

We focused on the anchors with embedment length larger than critical lengths, as the load shared by the embedded-end is lower in this case. As discussed before, from Eqn. (30), the reduction in bondline stiffness increases the load share at the embedded-end. Also, the stress distributions predicted considering the embedded-end fixed and free are similar, for such anchors. We employ the embedded-end condition as fixed to allow us to calculate the load-share at the embedded-end. In the first example, the analysis is carried out for anchor properties: $E = 210$ GPa and $d = 19$ mm, the bondline properties: $G_s = 1400$ MPa, $t = 1.6$ mm and $G_c = 0.5G_s$, and the embedment length $l = 177.8$ mm, adopting from Cook's work (see Table 1). For the baseline anchor with SBL, the fraction of load shared at the embedded-end p is calculated as 0.9%. A redistribution in the stresses along the bondline and a respective increase in the load share p is expected due to introduction of compliant phase. In order to study the effect of compliant phase on the stress-state in the bondline, a parametric study is carried out for anchors with DBL adhesive by varying the compliant bondlength ratio such that $\xi = \{0.1, 0.2, 0.3, 0.4\}$. The SBL anchor with stiff adhesive $G = G_s$ is chosen as the baseline case. Fig. 4 shows the comparison of adhesive shear stress distribution in super-critical-length anchors with SBL and DBL configurations. The maximum shear stress in the baseline anchor with SBL is $0.135(P/A)$ i.e. about 13.5% of tensile stress imposed on anchor rod. It is clearly seen that the peak stress in the bondline is reduced at the loaded-end when the DBL is employed in lieu of SBL owing to a favorable redistribution of shear stresses. For the DBL anchors with bondlength ratio $\xi > 0.2$, the peak stress is noted in the compliant phase of the bondline. Conversely, for DBL with $\xi < 0.2$, the peak shear stress is noted in the stiff adhesive phase. It is noted that a favorable distribution is the one in which the local peak stress in the stiff and the compliant phase are equal. Consequently, $\xi = 0.2$, gives the minimum value of peak shear stress for the choice of parameters chosen here. To better capture the benefit of grading, the bondline configuration has to be optimized by varying ξ and G_c.

As discussed before, for a given anchor, the inclusion of the complaint phase increases the load shared by the embedded-end. Therefore, in the next example, we parametrically identify the bondline configuration in order to reduce peak stress without significantly effecting the load-shared by the embedded-end. In first stage of parametric evaluation, analysis is carried out for the previous example by evaluating the variations in the peak stress and load share p as a function of modulus of compliant phase G_c and plotted in Fig. 5a. In this figure, the peak stress in the stiff phase, compliant phase and entire bondline can be seen. Note that for a smaller $G_c < 0.4G_s$, the peak stress is observed in the compliant phase and the peak stress shifts to stiff phase as the G_c increases beyond $0.4G_s$. For the parameters considered here, the optimal value of modulus of compliant adhesive is $0.4G_s$. In the next stage of parametric evaluation, using $G_c = 0.4G_s$ in the previous example, peak shear stress and the load share p are analyzed as function of compliant bondlength ratio ξ and plotted in Fig. 5b. From this figure, the peak stress is observed in the stiff phase for $\xi < 0.2$ and is observed in the compliant phase for $\xi > 0.2$. Therfore, for the anchor configuration considered here, the optimal values of shear modulus of compliant phase and the complaint bondlength ratio are $G_c = 0.5G_s$ and $\xi = 0.15$, respectively, with a peak stress of $0.0782(P/A)$. The optimal configuration leads to about 43% reduction in peak shear stress in comparison to anchor with SBL comprising stiff adhesive. Fig. 5a and b shows that the fraction of load shared by the embedded-end p decreases with the increase in modulus of compliant phase G_c and increases with the compliant bondlength ratio ξ which is expected. For the optimum anchor configuration, the load shared by the embedded-end was computed

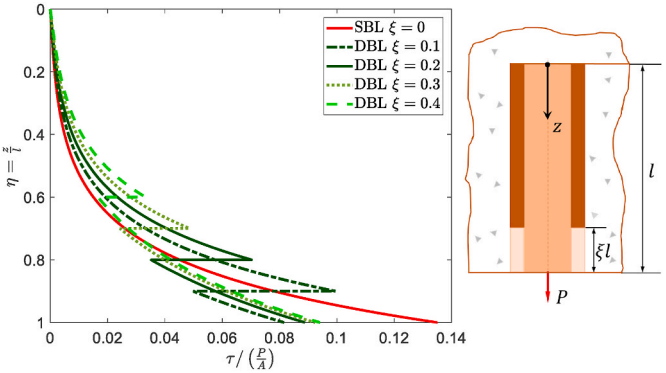

Fig. 4. DBL anchors with fixed embedded-end (Cook's super-critical anchor): The shear stress distribution at the mid-surface of the adhesive along embedment length for a choice of compliant bondlength ratio $\xi = \{0, 0.1, 0.2, 0.3, 0.4\}$ and $G_c = 0.5G_s$.

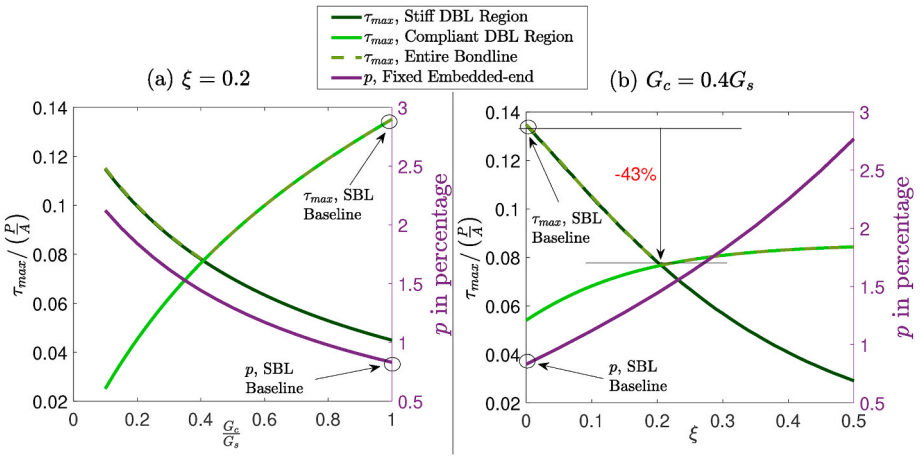

Fig. 5. DBL anchors with fixed embedded-end (Cook's super-critical anchor): Normalized peak shear stress in the stiff and the compliant phase of the adhesive as a function of (a) shear modulus mismatch between the compliant and stiff adhesives $\frac{G_c}{G_s}$ for $\xi = 0.2$ (b) compliant bondlength ratio ξ for $G_c = 0.4G_s$. Load shared by the embedded end is plotted on the vertical axis on the right.

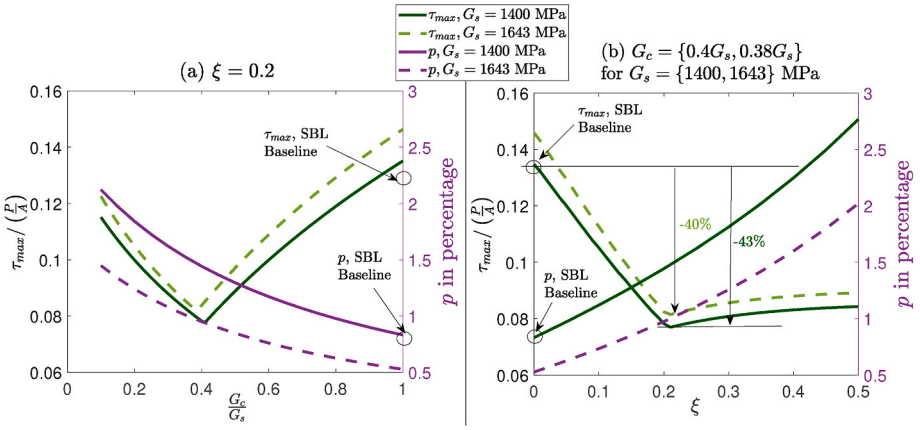

Fig. 6. DBL anchors with fixed embedded-end (Cook's super-critical anchor): Normalized peak shear stress in the stiff and the compliant phase of the adhesive as a function of (a) shear modulus mismatch between the compliant and stiff adhesives $\frac{G_c}{G_s}$ for $\xi = 0.2$ (b) compliant bondlength ratio ξ for $G_c = 0.4G_s$ and $0.38G_s$ for $G_s =$ 1400 and 1643 MPa, respectively. Load shared by the embedded-end is shown on the vertical axis on the right.

as 1.5% in comparison to 0.9% for the SBL anchor.

The percentage of load share that can be allowed at the embedded-end is left to the choice of designers and the proposed models could also be used to reduce the load share p by further stiffening of adhesive near the embedded-end in addition to the compliance imparted at the loaded-end. Fig. 6a and b repeats the parametric evaluation exercise by increasing the stiffness of the bondline in the stiff phase i.e., G_s is increased to 1643 MPa (corresponding to an adhesive with Young's modulus of 4600 MPa) and comparison is made against the previous parametric study. In these figures, it is clearly seen that increasing the modulus of stiffer adhesive reduces the load shared by the embedded end p for any configuration. However, this increase in stiffness leads to a greater value of the peak stress in the bondline in comparison to that of the optimal configuration.

In the next example, the idea of bondline tailoring is extended to multi-step variation in shear modulus of bondline adhesive to explore a possibility of further reduction in peak stress. The detailed parametric stress analysis of three adhesive bondline (TBL) system is discussed in appendix section 5.3. Fig. 7 illustrates the comparison of shear stress distribution obtained in anchors with SBL against those obtained for optimal DBL and TBL configurations. The bondlines based on parametric optimization for DBL and TBL adopted here are $\{G_c = 0.4G_s, \xi = 0.2\}$ and $\{G_{c1} = 0.4G_s, G_{c2} = 0.6G_s, \xi_1 = 0.1, \xi_2 = 0.2\}$, respectively. The baseline case for comparison is the SBL anchor with stiff adhesive G_s. In this figure, the redistribution of shear stress over a larger portion of the bondline is observed for TBL anchor in comparison to SBL or DBL bondlines. The peak stress reduction in case of TBL is 46% in comparison to the baseline anchor. Besides having a slightly greater influence on reducing the peak stress, the TBL anchor helps mitigate the load share at the embedded-end, originally introduced due to compliance tailoring. Due to higher practicability of the double-adhesive anchor implementation and its comparable performance in terms of peak shear stress reduction to TBL anchors, we advocate the use of DBL for anchors.

The proposed theory is applied to identify an optimal bondline configuration of the Boston tunnel anchor which is similar to the Cook's critical length anchors. The geometric and material properties chosen are: $l = 127$ mm, $d = 15.9$ mm, $E = 210$ GPa, $t = 1.6$ mm, $E_s = 3.92$ GPa, $\mu = 0.4$. Fig. 8a and b shows the axial stress distribution in the anchor and shear stress distribution in bondline, respectively, for four different cases: 1. Baseline SBL with $G_s = 1400$ MPa, 2. Stiffer SBL with $G_s = 1643$ MPa (corresponding to a Young's modulus of 4.6 GPa), 3. DBL parametrically optimized for minimizing peak shear stress and 4. DBL

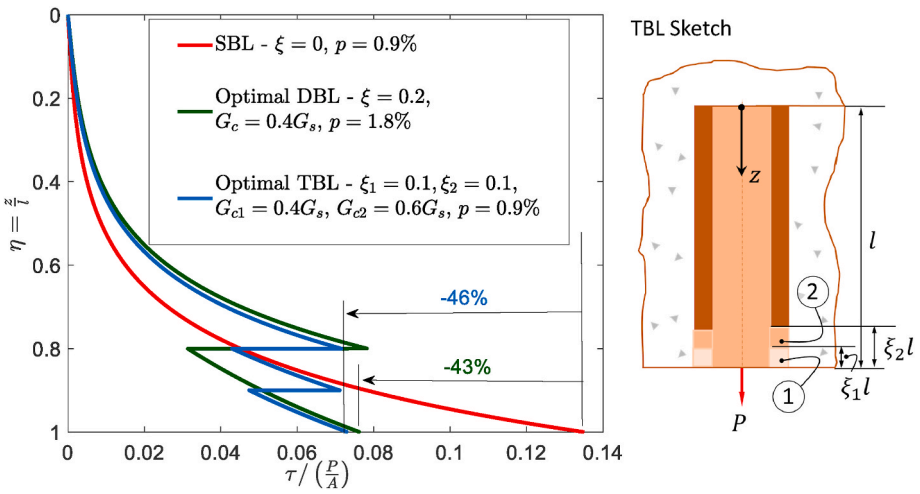

Fig. 7. Multiple-adhesive anchors (Cook's super-critical anchor): Comparison of normalized shear stress distribution in the optimal DBL and TBL anchors with SBL anchor.

parametrically optimized for retaining the load shared by the embedded-end. The cases 2 and 4 are obtained by employing a stiffer bondline, with modulus greater than the original problem. The detailed parametric plots showing the peak stresses as a function of adhesive compliance and the bondlength ratios are presented and discussed in appendix. From Fig. 8a, we can clearly see that the axial stress at the embedded end is increased as we increase the compliance of the bondline, however, the axial stress at the embedded-end does not increase when we stiffen the original bondline by increasing G_s from 1400 to 1643 MPa. Note that the axial stress is a function of load shared at this end. The anchor used for the ceiling of the Boston tunnel has a load share of 2.7% at the embedded-end. Note that for an anchor with SBL, an increase in modulus of the bonline leads to higher stress peaks at the loaded-end. The first attempt to perform parametric optimization was carried out by purely tailoring the compliance of the bonline leading to a reduction in peak stress of 38% as seen in Fig. 7. Due to the increased compliance obtained by replacing 20% of bondline by adhesive of shear modulus $= 0.48G_s$, the load share at the embedded-end increased up to 4%. In the second attempt to perform parametric optimization, the stiffness near the embedded-end was increased to $G_s = 1643$ MPa and the parametric optimization was performed by maintaining the load share at the embedded-end $p = 2.7\%$. In this attempt, the reduction in peak stress was about 27%, however, the stress condition of the original anchor was unaltered. The adhesive tailoring could be more effective for

Table 2
Load-shared by the embedded-end, calculated using the approximate formula: $p = \text{sech}((\alpha_c\xi + \alpha_s(1-\xi))l)$ and checking error against the proposed model solution for p.

Farmer's Configuration: $G_s = 804$ MPa, $G_c = 402$ MPa, E = 180 GPa							
L mm	d mm	t mm	ξ	k_l	p_{approx}	p_{actual}	%age Error in p
350	20	4	0	5.73	0.007	0.007	0.000
350	20	4	0.1	5.56	0.008	0.008	8.129
350	20	4	0.2	5.39	0.009	0.010	11.745
350	20	4	0.3	5.22	0.011	0.012	13.350
350	20	4	0.4	5.06	0.013	0.015	14.056
350	20	4	0.5	4.89	0.015	0.018	14.342
175	20	4	0.2	2.70	0.134	0.146	8.011
87.5	20	4	0.2	1.35	0.487	0.507	4.107
Cook's Configuration: $G_s = 1400$ MPa, $G_c = 700$ MPa, $E = 210$ GPa							
L mm	d mm	t mm	ξ	k_l	p_{approx}	p_{actual}	%age Error in p
177.8	19	1.6	0	5.48	0.009	0.009	0.000
177.8	19	1.6	0.1	5.32	0.010	0.011	7.900
177.8	19	1.6	0.2	5.16	0.011	0.013	11.536
177.8	19	1.6	0.3	5.00	0.013	0.016	13.207
177.8	19	1.6	0.4	4.84	0.016	0.018	13.965
177.8	19	1.6	0.5	4.68	0.019	0.022	14.280
127	16	1.6	0	4.30	0.027	0.027	0.000
127	16	1.6	0.1	4.17	0.031	0.033	6.666
127	16	1.6	0.2	4.05	0.035	0.039	10.289

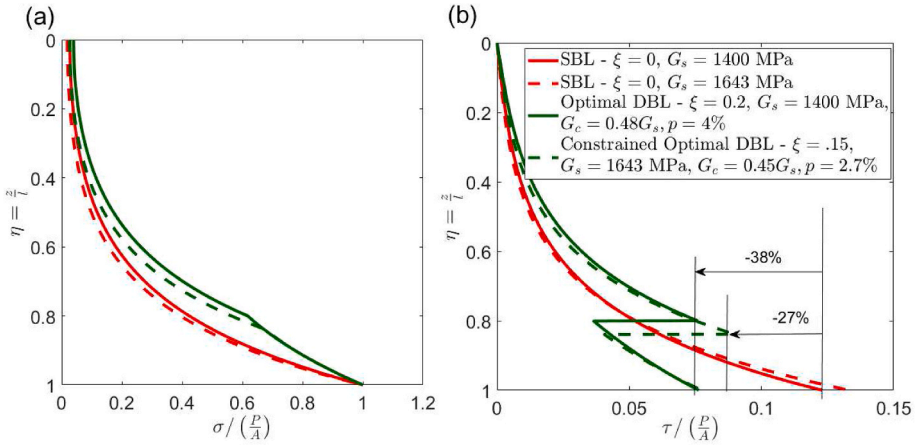

Fig. 8. Boston Tunnel Anchor (Cook's Critical-length anchor): Comparison of (a) axial stresses and (b) shear stresses, in the optimal DBL anchors against the SBL anchor baseline. The constrained optimal DBL corresponds to the case where the load share at the embedded-end is kept constant while performing optimization. The legend is the same for both sub-plots.

critical length anchors (Boston tunnel configuration) when we stiffen the bondline near the embedded-end.

Utilizing the proposed theory, as discussed before, the closed form formulas are obtained for the peak stresses in the bondline and load shared by the embedded-end. A simplified yet approximate formula for the load shared by the embedded end of a DBL anchor is proposed by treating it as an equivalent SBL anchor with the constant $\alpha_{eff} = \alpha_c + \alpha_s(1 - \xi)$, where, $\alpha_c = \sqrt{\frac{\pi(d+t)G_c}{EAt}}$ and $\alpha_s = \sqrt{\frac{\pi(d+t)G_s}{EAt}}$. The load shared by the embedded-end could be approximately computed as

$$p = sech(\alpha_{eff} l) \tag{38}$$

This formula is implemented for some anchor configurations in Table 2, and noted an error up to about 15%. However, the error is found to be larger for configuration with larger p values and decreases with a decrease in p value.

4. Conclusions

A simple linear elastic theoretical framework for anchors is developed and used to analyze the stress reduction potential, including the consideration of the constraint of maintaining the critical length of the design. Closed-form solution and algebraic equations based on shear-lag analyses are presented for the anchors with double-adhesive and multiple-adhesive bondlines, respectively, to predict the shear stresses in the bondline and the load shared by the embedded-end. The closed-form solution is validated using the results obtained from an analogous finite element model and an extant study. The compliance tailoring of the bondline in bonded anchors can reduce the maximum stresses driving failure by as much as 43% for the simplest double-adhesive tailoring, without significantly influencing the stress-state at the embedded-end. An example of super-critical-length anchors with n-adhesive bondline indicates that the peak stresses could be reduced by about 46% by using three adhesives along the bondline, in lieu of a single adhesive, without significantly loading the embedded-end. A marginal improvement in peak stress reduction for the case of bondline with three adhesives in comparison to double-adhesive bondline and practical considerations of deploying multiple adhesives, advocate the use of latter. The following observations are drawn based on the stress-transfer characteristics of double-adhesive bondline and triple adhesive bondline anchors:

- The load-transfer from anchor to the matrix through the adhesive could be more uniform and the peak stresses could be shifted away from the loaded-end, if multiple adhesives representing a step-wise variation in shear modulus of the bondline is considered in lieu of a single adhesive bondline.
- The compliance tailoring demonstrated here with the help of double-adhesive or n-adhesives is more suitable for the anchors with larger embedment depths.
- For double-adhesive anchors, the peak adhesive shear stress and the location at which it occurs along the bondline is dependent on the compliant bondlength ratio and the modulus of compliant phase with respect to the modulus of stiff phase.
- An approximate yet simplified formula for evaluating the load shared by the embedded-end is proposed.

However, gradual creep softening and damage needs to be accounted for, to accurately predict the creep failure. Therefore, creep failure analysis of tailored adhesive anchors is left to a subsequent study.

Acknowledgment

S. K would like to thank the university of Glasgow for the start-up grant (Award No: 144690-1). M. A. K wants to thank Mahindra University for funding internal research project on the development of high performance geopolymer concrete.

Appendix

Finite Element (FE) Model

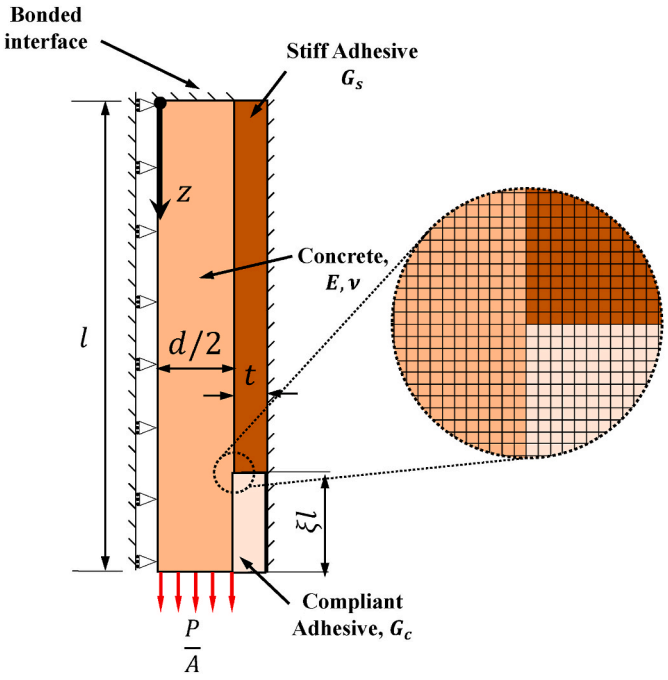

Fig. A1. Axisymmetric Model: FE mesh, loading and boundary conditions for the anchor with bonded embedded-end.

To perform the validation of the solutions obtained for the anchors with SBL and DBL, finite element analyses was performed on an adhesively bonded anchor assembly shown in Fig. 1b by treating the embedded-end as fixed and free. The analyses was performed using ABAQUS 6.14 code. A 3D axisymmetric FE model, shown in Fig. A1, was set up with loading and boundary conditions representing anchor assembly fully bonded to the concrete substructure i.e., perfect bonding of cylindrical bondline with both the concrete and the anchor core, transferring the load through shearing. The tensile load is applied as a traction at the bottom surface of the anchor core. As the concrete substrate is semi-infinite, it is considered to be rigid. The properties of the steel and the bondline adhesive are same as that of the analytical model. Due to restraint by rigid concrete, the bondline was fixed along the outer periphery at $(d/2 + t)$. The embedded-end condition was chosen as fixed or free depending on the case to be validated. The adhesive is divided into two phases representing compliant and stiff regions, akin to schemata of analytical model. A 4-noded bi-linear axi-symmetric quadrilateral element (CAX4R) with radial and axial degrees of freedoms at each node was used to mesh the entire geometry. The mesh size of 0.1 mm $\times$ 0.1 mm was chosen based on a sensitivity analysis for both the anchor and the adhesive. A linear static analysis was performed and the shear stress at the mid-surface of the bondline was extracted for comparison with the analytical model.

Critical-length Characteristics of Adhesive Anchor

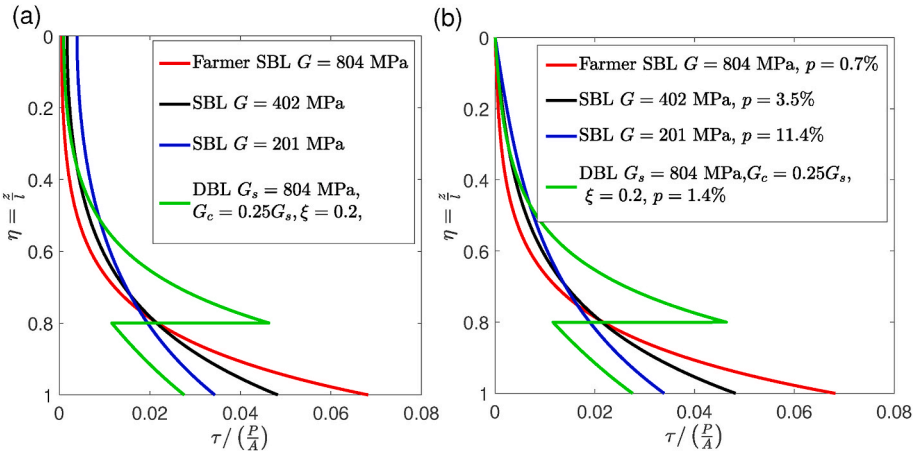

Fig. A2. Effect of shear stiffness of adhesive on p with SBL and DBL super-critical length anchors: Normalized adhesive shear stress along the bondline as a function of adhesive modulus G for SBL anchors and its comparison against the DBL anchor for super-critical-length anchors for (a) Embedded-end free and (b) Embedded-end fixed; for DBL, $G_c = 0.25G_s$, $\xi = 0.2$, $l = 350$ mm.

The critical-length characteristic of an anchor configuration is sensitive to the shear stiffness of bondline as noted in Eqn. (30). We choose to verify this by analyzing an anchor from Farmer's work as we have used it for validation of the proposed models. The baseline case for DBL anchor configuration is taken as ($E = 180$ GPa, $d = 20$ mm, $G_s = 804$ MPa, $t = 4$ mm, $G_c = 0.5G_s$, $l = 350$ mm, $\xi = 0.25$). The SBL baseline is chosen by changing the bondline configuration to $G = G_s = 804$ MPa. First, we study the effect of modulus of adhesive on the critical length characteristic of anchor. It is important to reiterate that the critical-length of the anchor is the minimum length required for shear-dominated load tranfer, identified by zero shear stress (negligible) at the embedded-end. Fig. A2a, depicts the shear stress distributions along the bondline of the SBL anchors for choices of shear modulus of adhesive $G = \{804, 402, 201\}$ MPa for the anchors with free embedded-end. Note that, for the anchor with ($G = 804$ MPa), the shear stress vanishes near the embedded-end, while it increases with the decrease in shear modulus of the SBL. Therefore, the critical length characteristic is lost with the increase in shear modulus of the adhesive. Note that the shear stress is always zero at the embedded-end for the anchor with fixed embedded-end. However, the load share by the embedded-end is zero (negligible) for the critical length anchors with fixed embedded-end. The non-zero shear stress at the embedded-end for the anchor with free embedded-end is manifested by the load share/the axial stress at the embedded-end for the anchor with fixed embedded-end. We particularly emphasize on load share instead of axial stress at the embedded-end due to uncertainty associated with the fixity at the embedded-end, depending on the amount of adhesive reaching this end. From Eqn. (9), the shear stress at the embedded-end is a function of $1/\sinh(l)$ and therefore, increases with the decrease in embedment depth. The critical-length parameter $k_l = \alpha l$ for the present joint configuration (with $G = 804$ MPa) is calculated as 4.314. The SBL anchors with $k_l < 4.314$ does not show complete load transfer in shear. Most of the configurations reported in Table 1, focused on designs whose k_l is greater than 4.3.

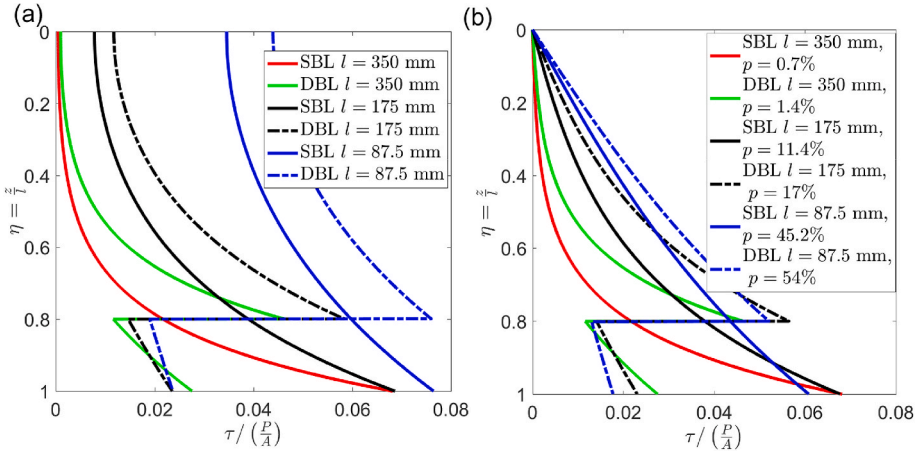

Fig. A3. Effect of embedment depth l on p with SBL and DBL super-critical length anchors: Shear stress distribution along the length of the SBL and DBL anchors for a choice of embedment length $l = \{350, 175, 87.5\}$ mm for (a) Embedded-end free and (b) Embedded-end fixed; for DBL, $G_c = 0.25G_s$, $\xi = 0.2$.

Now, we are interested in looking at effect of embedment length on the critical-length characteristics of the anchor SBL and the DBL anchors. As noted before, the loss of critical length characteristic is observed, either in terms of magnitude of the shear stress in the bondline at the embedded-end for the anchor with free embedded-end or in terms of load share at the embedded-end for the anchor with fixed embedded-end. Figs. A3a and A3b, shows the shear stresses along the bondline for the SBL and DBL anchors for the choice of embedment depth $l = \{350, 175, 87.5\}$ mm. For comparison, farmer's SBL and DBL configurations are chosen as baselines. It can be clearly seen that the decrease in the embedment depth of the bondline leads to a greater load share at the embedded-end for both the SBL and DBL anchors leading to loss of critical length characteristic. Note that we are using only the fixed embedded-end condition to analyze the adhesive anchors in all the remaining sections of the paper.

Parametric Optimization of Cook's Supercritical TBL Anchor

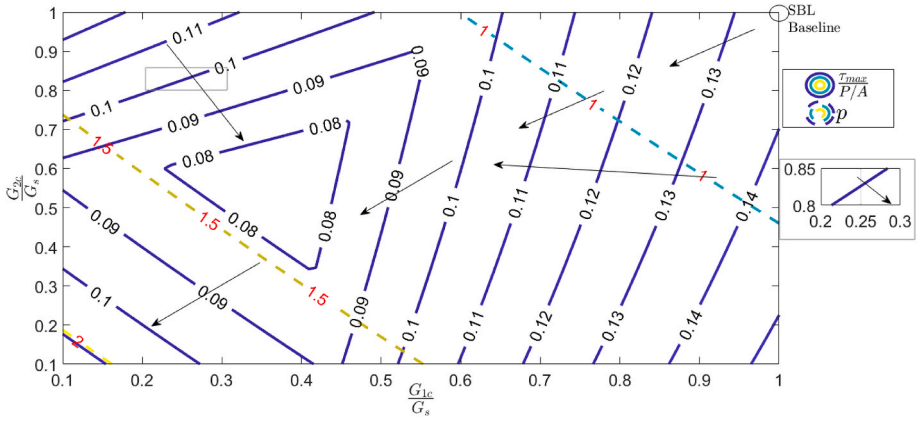

Fig. A4. TBL anchors (Cook super-critical): The solid lines depicts the peak shear stress drawn as a contour plot as a function of moduli of compliant phases $\{G_{c1}, G_{c2}\}$ for $\xi_1 = 0.1$ and $\xi_2 = 0.2$. The dashed lines shows the load shared by the embedded-end as a contour plot as a function of moduli of compliant phases $\{G_{c1}, G_{c2}\}$.

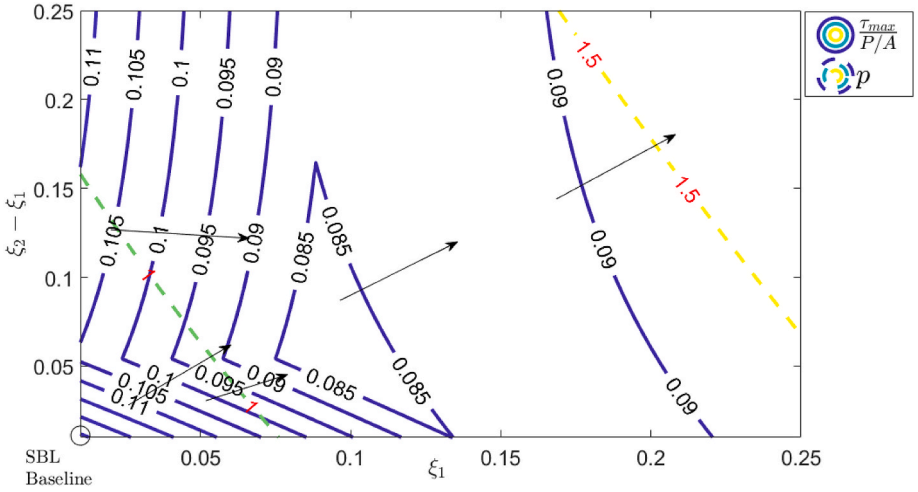

Fig. A5. TBL anchors (Cook super-critical): The solid lines depicts peak shear stress drawn as a contour plot as a function of compliant bondlength ratios $\{\xi_1, \xi_2 - \xi_1\}$; for $G_{c1} = .4G_s$ and $G_{c2} = .6G_s$. The dashed lines shows the load shared by the embedded-end as a contour plot as a function of compliant bondlength ratios ξ_1, ξ_2.

The analysis is carried out choosing anchor properties as ($E = 210$ GPa, $d = 19$ mm), the bondline configuration as ($G_s = 1400$ MPa, $t = 1.6$ mm), and the embedment depth $l = 177.8$ mm, adopted from Cook's work (see Table 1). The solution developed for the n-adhesive bondline will be used here. For coherence of discussions, we denote $G_{ci} = G_i$ for $n < i$ i.e., multiple compliant phases and $G_n = G_s$ for the stiff phase near the embedded-end. The bondline configuration has to be optimized such that the load share at the embedded-end is not significantly influenced. We choose anchor with three-adhesive bondline denoted here as TBL anchor which contains two complaint phases and one stiff phase along the bondline. Fig. A4 shows the peak shear stress $\tau_{\max}$ and the load share p as a contour plot of modulii of compliant phases $\{G_{c1}, G_{c2}\}$ ranging between $0.1G_s$ to G_s. In this figure, the solid arrows indicate how the optimum could be approach by reducing the shear moduli and dashed arrow indicates the distribution of p as a function of compliance. The loss in p could also be mitigated by employing more stiff adhesive in region near the embedded-end, i.e., order of modulus of adhesive should be $G_s > G_{c2} > G_{c1}$. Also observe from the inset that G_{c2} should be greater than G_{c1} by about 1.27 times, looking at the direction of top left arrow. Note that the load share p is within 2% for $\{G_{c1}, G_{c2}\} = \{0.4G_s, 0.6G_s\}$.

In the next stage of a parametric optimization, by fixing $\{G_{c1}, G_{c2}\} = \{0.4G_s, 0.6G_s\}$, the peak stress is minimized as a function of compliant bondlength ratios $\{\xi_1, \xi_2 - \xi_1\}$, while simultaneously observing the load share by the embedded-end p, as demonstrated by Fig. A5. Note that for the values of ξ_1 and/or $(\xi_2 - \xi_1)$ greater than 0.25, the peak shear stress calculated is greater than the maximum value. From Fig. A5, note that for $\xi_1 = 0.1$, $\xi_2 - \xi_1$ can be chosen between 0.05 and 0.1 without significantly altering peak shear stress. The dashed lines shows the load shared by the embedded-end as a contour plot as a function of compliant bondlength ratios $\{\xi_1, \xi_2 - \xi_1\}$. The solid arrows indicate how the optimum could be approach by reducing the shear moduli and dashed arrow indicates the trend of p as we add more compliance. Note that here while approaching the optimal solution, the bondlength ratio of second phase i.e., $\xi_2 - \xi_1$ should be about 0.75–1 times the bondlength ratio closer to loading i.e., ξ_1, looking at the direction of bottom solid arrow. Therefore, for brevity, we choose $\{\xi_1, \xi_2 - \xi_1\} = \{0.1, 0, 1\}$ as the optimal compliant bondlength ratios, leading to a reduction of about 46% in the peak bondline stresses. The load share by the embedded-end for the optimal bondline configuration is about 1.1%.

Parametric Optimization of Boston Tunnel Anchor

The cook critical configuration is similar to the anchor in the Boston tunnel. The parameteric optimization of the Boston tunnel anchor configuration is depicted in the Figs. A6 and A7. Fig. A6 shows the parametric optimization for minimizing the peak stresses by reducing the compliance of the bondline near the loaded-end in two stages. In the first stage, the peak stress is minimized in relation to the stiffness of the compliant phase G_c, at a constant compliant bonlenght ratio ξ. In the subsequent stage, the peak stress is minimized in relation to the compliant bondlength ratio ξ, for the fixed G_c, obtained in the previous stage. The optimal bondline which reduces the peak shear stress by about 38% is $\xi = 0.2$ and $G_c = 0.48G_s$. Fig. A7 shows an additional parametric sweep for the anchor whose bondline is stiffened to reduce the load share at the embedded-end. In this case, we search for a bondline configuration such that the load share at the embedded-end is the same as the original SBL anchor. It can be seen that the parameters $G_c = \xi = 0.15$, $G_c = 0.45G_s$ corresponds to $p = 2.7\%$ with a reduction in peak stress about 34%.

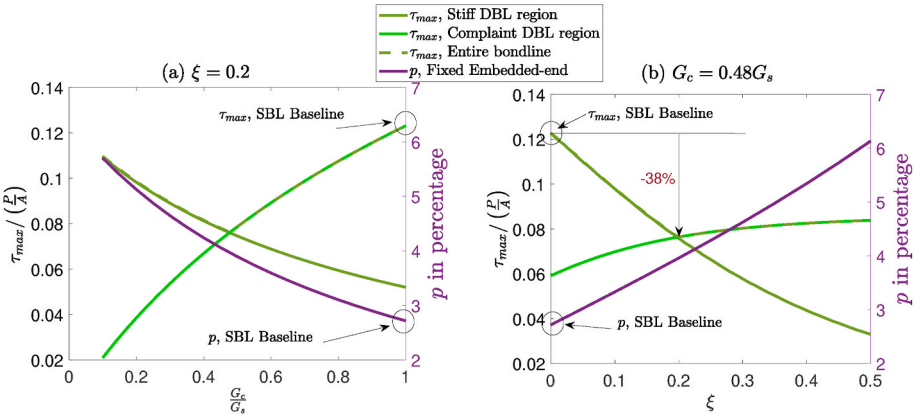

Fig. A6. DBL anchors with fixed embedded-end (Cook critical anchor): Peak shear stress in the stiff and the compliant phase of the adhesive as a function of (a) modulus of compliant adhesive in relation to stiff adhesive $\frac{G_c}{G_s}$ for $\xi = 0.2$ (b) compliant bondlength ratio ξ for $G_c = 0.48G_s$. Load shared by the embedded end is plotted on the vertical axis on the right.

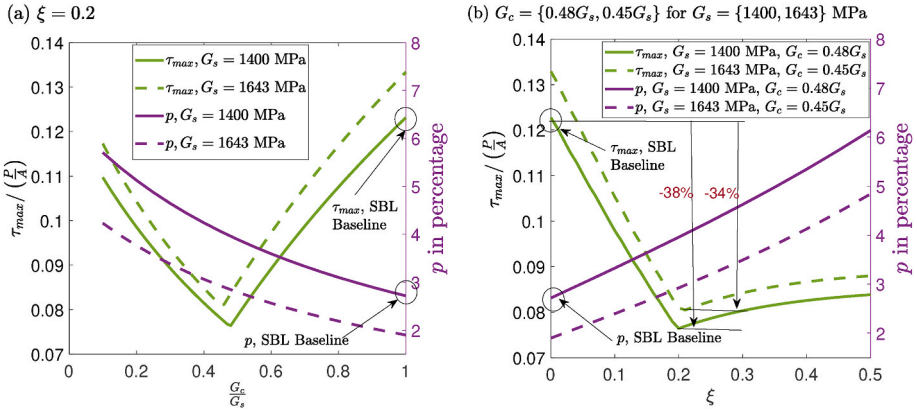

Fig. A7. DBL anchors with fixed embedded-end (Cook super-critical anchor): Peak shear stress in the stiff and the compliant phase of the adhesive as a function of (a) modulus of compliant adhesive in relation to stiff adhesive $\frac{G_c}{G_s}$ for $\xi = 0.2$ (b) compliant bondlength ratio ξ for $G_c = 0.48G_s$ and $0.45G_s$ for $G_s = 1400$ and 1643 MPa, respectively. Load shared by the embedded end is plotted on the vertical axis on the right.

References

[1] Pablo A Prieto-Muñoz, Huiming M Yin, and Rene B Testa. Mechanics of an adhesive anchor system subjected to a pullout load. ii: viscoelastic analysis. J Struct Eng, 140 (2): , 2013.

[2] Contrafatto Loredana, Cosenza Renato. Behaviour of post-installed adhesive anchors in natural stone. Construct Build Mater 2014;68:355–69.

[3] Eligehausen Rolf, Cook Ronald, Appl Jorg. Behavior and design of adhesive bonded anchors. ACI Struct J 2006;103(6):822–32.

[4] Çolak Adnan. Parametric study of factors affecting the pull-out strength of steel rods bonded into precast concrete panels. Int J Adhesion Adhes 2001;21(6): 487–93.

[5] Cook Ronald A. Behavior of chemically bonded anchors. J Struct Eng 1993;119(9): 2744–62.

[6] RA Cook, GT Doerr, and RE Klingner. Bond stress model for design of adhesive anchors. ACI Struct J, 90(5), 1993.

[7] Ahmed Ehab A, El-Salakawy Ehab F, Benmokrane Brahim. Tensile capacity of gfrp postinstalled adhesive anchors in concrete. J Compos Construct 2008;12(6): 596–607.

[8] Zavliaris KD, Kollias S, Speare PRS. An experimental study of adhesively bonded anchorages in concrete. Mag Concr Res 1996;48(175):79–93.

[9] National Transportation Safety Board (NTSB). Ceiling collapse in the interstate 90 connector tunnel boston Massachusetts, july 10, 2006. Tech Rep 2007.

[10] Kumar S, Khan MA. A shear-lag model for functionally graded adhesive anchors. Int J Adhesion Adhes 2016;68:317–25.

[11] Upadhyaya Priyank, Kumar S. Pull-out capacity of adhesive anchors: an analytical solution. Int J Adhesion Adhes 2015;60:54–62.

[12] Chaallal Omar, Benmokrane B. Pullout and bond of glass-fibre rods embedded in concrete and cement grout. Mater Struct 1993;26(3):167–75.

[13] Yilmaz Salih, Ali Özen Muhammet, Yardim Yavuz. Tensile behavior of post-installed chemical anchors embedded to low strength concrete. Construct Build Mater 2013;47:861–6.

[14] Çalışkan Özlem, Yılmaz Salıh, Kaplan Hasan, Kıraç Nevzat. Shear strength of epoxy anchors embedded into low strength concrete. Construct Build Mater 2013;38: 723–30. 25th Anniversary Session for ACI 228 – Building on the Past for the Future of NDT of Concrete.

[15] Azizinamini A, Chisala M, Ghosh SK. Tension development length of reinforcing bars embedded in high-strength concrete. Eng Struct 1995;17(7):512–22.

[16] McVay Michael, Cook Ronald A, Krishnamurthy Kailash. Pullout simulation of postinstalled chemically bonded anchors. J Struct Eng 1996.

[17] Farmer IW. Stress distribution along a resin grouted rock anchor. Int J Rock Mech Min Sci Geomech Abstracts 1975;12(11):347–51.

[18] Seo Jin Kim, Scott T. Smith. Pullout strength models for frp anchors in uncracked concrete. J Compos Construct 2010;14(4):406–14.

[19] Wang Yan-Jie, Wu Zhi-Min, Zheng Jian-Jun, Yu Rena C, Zhou Xiang-Ming. Three-dimensional axisymmetric analytical method for pull-out behaviour of adhesive anchors in concrete. Eng Fract Mech 2020;226:106876.

[20] Zaeri Ahmad Reza, Saeidi Googarchin Hamed. Analysis of automotive mixed-adhesive joints weakened by moist conditions: experimental characterization and numerical simulation using cohesive zone model. Fatig Fract Eng Mater Struct 2019;42(4):929–42.

[21] Li Fei, Zhao Qi Lin, Chen Hao Sen, Wang Jin Quan, Duan Jing Hui. Prediction of tensile capacity based on cohesive zone model of bond anchorage for fiber-reinforce dpolymer tendon. Compos Struct 2010;92(10):2400–5.

[22] Malachanne Etienne, Jebli Mouad, Jamin Frederic, Garcia-Diaz Eric, El Youssoufi Moulay-Said. A cohesive zone model for the characterization of adhesion between cement paste and aggregates. Construct Build Mater 2018;193:64–71.

[23] Cook Ronald A, Konz Robert C. Factors influencing bond strength of adhesive anchors. ACI Struct J 2001;98(1).

[24] Doerr GT, Klingner RE. Adhesive anchors: behavior and spacing requirements. Technical report; 1989. interim report.

[25] Chen Jianhang, Saydam Serkan, Paul C, Hagan. An analytical model of the load transfer behavior of fully grouted cable bolts. Construct Build Mater 2015;101: 1006–15.

[26] Zheng Jian-Jun, Dai Jian-Guo. Analytical solution for the full-range pull-out behavior of frp ground anchors. Construct Build Mater 2014;58:129–37.

[27] Prieto-Muñoz Pablo A, Yin Huiming M, Rene B Testa. Mechanics of an adhesive anchor system subjected to a pullout load. i: elastic analysis. J Struct Eng 2013.

[28] Tipireddy R, Kumar S. Spatially-degraded adhesive anchors under material uncertainty. Int J Adhesion Adhes 2017.
[29] Stapleton Scott E, Waas Anthony M, Arnold Steven M. Functionally graded adhesives for composite joints. Int J Adhesion Adhes 2012;35:36–49.
[30] da Silva Lucas FM, Lopes Maria João CQ. Joint strength optimization by the mixed-adhesive technique. Int J Adhesion Adhes 2009;29(5):509–14.
[31] Pires I, Quintino L, Durodola JF, Beevers A. Performance of bi-adhesive bonded aluminium lap joints. Int J Adhesion Adhes 2003;23(3):215–23.
[32] Kumar S, Adams Robert D. Special issue on functionally graded adhesively bonded systems. 2017.
[33] Carbas RJC, Da Silva LFM, Critchlow GW. Adhesively bonded functionally graded joints by induction heating. Int J Adhesion Adhes 2014;48:110–8.
[34] Stapleton Scott E, Julia Weimer, Jan Spengler. Design of functionally graded joints using a polyurethane-based adhesive with varying amounts of acrylate. Int J Adhesion Adhes 2017;76:38–46 [Special Issue on Functionally Graded Materials].
[35] Khan MA, Kumar S, Reddy JN. Material-tailored adhesively bonded multilayers: a theoretical analysis. Int J Mech Sci 2018;148:246–62.
[36] Khan MA, Kumar S. Performance enhancement of tubular multilayers via compliance-tailoring: 3d printing, testing and modeling. Int J Mech Sci 2018;140:93–108.
[37] Khan MA, Kumar S, Cantwell Wesley J. Additively manufactured cylindrical systems with stiffness-tailored interface: modeling and experiments. Int J Solid Struct 2018;152:71–84.
[38] Kumar S, Wardle Brian L, Arif Muhamad F. Strength and performance enhancement of bonded joints by spatial tailoring of adhesive compliance via 3d printing. ACS Appl Mater Interfaces 2017;9(1):884–91. PMID: 27966344.
[39] Kumar Shanmugam, Wardle Brian L, Arif Muhamad F, Ubaid Jabir. Stress reduction of 3d printed compliance-tailored multilayers. Adv Eng Mater 2018;20(1):1700883.
[40] Ubaid Jabir, Wardle Brian L, Kumar Shanmugam. Strength and performance enhancement of multilayers by spatial tailoring of adherend compliance and morphology via multimaterial jetting additive manufacturing. Sci Rep 2018;8(1):1–10.
[41] Dugbenoo Edem, Arif Muhamad F, Wardle Brian L, Kumar Shanmugam. Enhanced bonding via additive manufacturing-enabled surface tailoring of 3d printed continuous-fiber composites. Adv Eng Mater 2018;20(12):1800691.
[42] Cook RA, Fagundo FE, Biller MH, De Richardson. Tensile behavior and design of single adhesive anchors. Struct Mater Res Rep 1991;(91–3).
[43] Pablo A Prieto-Muñoz, Huiming M Yin, and Rene B Testa. Mechanics of an adhesive anchor system subjected to a pullout load. i: elastic analysis. J Struct Eng, 140(2): 2013.
[44] Prieto-Muñoz Pablo A, Yin Huiming M, Rene B Testa. An elastic analysis that predicts the pull-out capacity of adhesive anchors. In: IOP conference series: materials science and engineering, 10. IOP Publishing; 2010, 012151.
[45] Cusens AR, Yu Z. Pullout tests of epoxy-coated reinforcement in concrete. Cement Concr Compos 1992;14(4):269–76.
[46] Kumar S, Mittal KL, editors. Advances in modeling and design of adhesively bonded systems. John Wiley & Sons; 2013.
[47] Kumar S, Khan MA. An elastic solution for adhesive stresses in multi-material cylindrical joints. Int J Adhes Adhes 2016;64:142–52.